

Central exclusive diffractive production of two-pion continuum at hadron colliders

R.A. Ryutin ^{a,1}

¹Institute for High Energy Physics, NRC “Kurchatov Institute”, Protvino 142 281, Russia

July 28, 2019

Abstract Calculations of the central exclusive diffractive di-pion continuum production are presented in the Regge-eikonal approach. Data from ISR, STAR, CDF and CMS were analysed and compared with theoretical description. We also consider theoretical predictions for LHC, possible nuances and problems of calculations and prospects of investigations at present and future hadron colliders.

PACS 11.55.Jy Regge formalism · 12.40.Nn Regge theory, duality, absorptive/optical models · 13.85.Ni Inclusive production with identified hadrons · 13.85.Lg Total cross sections

Introduction

In previous papers [1],[2] general properties and calculations of the Central Exclusive Diffractive Production (CEDP) were considered. It was shown, especially in [2], that diffractive patterns (differential cross-sections) of CEDP play significant role in model verification.

Here we partially continue the subject of [2] and investigate in detail the process of low mass CEDP (LM CEDP) with production of two pions. This process is one of the “standard candles” for LM CEDP. Why do we need exact calculations and predictions for this process?

- Di-pion LM CEDP is the basic background process for CEDP of resonances (like f_2 or f_0), since one of the basic hadronic decay mode for these resonances is the two pion one.
- We can use LM CEDP to fix the procedure of calculations of “rescattering” (unitarity) corrections. In the case of di-pion LM CEDP there are two kinds

of corrections, in the proton-proton and the pion-proton subamplitudes. They will be considered in the present work.

- Pion is the most fundamental particle in the strong interactions, and LM CEDP gives us the powerful tool to go deep inside its properties, especially, investigate the form factor and scattering amplitudes for the off-shell pion.
- LM CEDP has rather large cross-sections. It is very important for an exclusive process, since in the special low luminosity runs (of the LHC) we need more time to get enough statistics.
- As was proposed in [3], it is possible to extract some reggeon-hadron cross-sections. In the case of single and double dissociation it was the Pomeron-proton one. Here, in the LM CEDP of the di-pion we can analyze properties of the Pomeron-Pomeron to pion-pion exclusive cross-section, and also check again predictions of the covariant reggeization method [3].
- Diffractive patterns of this process are very sensitive to different approaches (subamplitudes, form factors, unitarization, reggeization procedure), especially differential cross-sections in t and ϕ_{pp} (azimuthal angle between final protons), and also $M_{\pi\pi}$ dependence. That is why this process is used to verify different models of diffraction.
- All the above items are additional advantages provided by the LM CEDP of two pions, which has usual properties of CEDP: clear signature with two final protons and two large rapidity gaps (LRG) [4],[5] and the possibility to use the missing mass method [6].

Processes of the LM CEDP were calculated in some other works [7]-[12] which are devoted to most popular models for the LM CEDP of di-mesons. All authors have considered nonperturbative approach in Reggeon-

^ae-mail: Roman.Rioutine@cern.ch

Reggeon collision subprocess. For example, in the Durham model [7]-[9] (see Fig. 1), they take the Born Regge term for the amplitude of the process $p + p \rightarrow p + \pi^+ + \pi^- + p$ with reggeized propagator of the off-shell pion, then they take into account unitarity (rescattering) corrections (in the initial proton-proton state and also in so-called “enhanced” one). In articles [10]-[12] authors do not introduce “enhanced” corrections, but take into account pion-proton interactions in the final state (see Fig. 2). There are some inconsistencies in this approach: complicated formula, which mix reggeized and bare off-shell pion propagators, and also mix a partially Regge approach with complex spin and a model with fixed “Pomeron spin” (vector or tensor Pomeron).

In this article we consider several cases, depicted in Fig. 3, and show how they describe the data from ISR [13],[14], STAR [15],[16], CDF [17],[18], CMS [19],[20] collaborations.

In the first part of the present work we introduce the framework for calculations of double pion LM CEDP (kinematics, amplitudes, differential cross-sections) in the Regge-eikonal approach.

In the second part we analyse the experimental data on the process at different energies, find the best approach and make some predictions for LHC experiments.

In the final part we discuss possibilities to extract Pomeron-Pomeron cross-sections from the data and analyse the present situation. Also we show some nuances of the calculations, which we should take into account (elastic amplitudes for virtual particles, off-shell pion form factor, pion-pion elastic amplitude at low energies, nonlinearity of the pion trajectory).

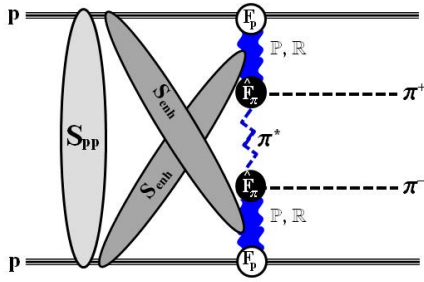


Fig. 1 Amplitude of the process of double pion LM CEDP $p + p \rightarrow p + \pi^+ + \pi^- + p$ in the KMR approach [7]-[9]. Central part of the diagram is the Born amplitude (with Pomeron and two reggeons). Reggeized off-shell pion propagator is shown as a dashed zigzag line. Proton-proton rescattering is depicted as S_{pp} -blob, and “enhanced” corrections are also shown as S_{enh} -blob. Off-shell pion form factor is presented as a black circle.

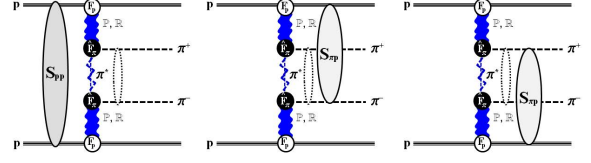


Fig. 2 Amplitude of the process of double pion LM CEDP $p + p \rightarrow p + \pi^+ + \pi^- + p$ in the approach [10]-[12]. Central part of the diagram is the Born amplitude (with Pomeron and two reggeons). Mixture of reggeized and bare off-shell pion propagators is shown as a dashed zigzag line plus dashed straight line. Proton-proton rescattering is depicted as S_{pp} -blob, and pion-proton rescattering corrections are also shown as $S_{\pi p}$ -blobs. Off-shell pion form factor is presented as a black circle.

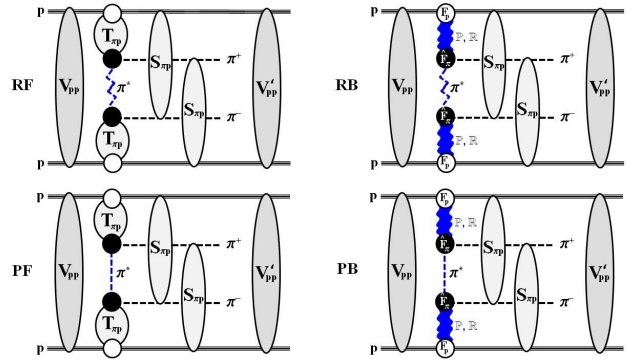


Fig. 3 Amplitude of the process of double pion LM CEDP $p + p \rightarrow p + \pi^+ + \pi^- + p$ in the Regge-eikonal approach for different cases. PB: central part of the diagram is the Born amplitude (with Pomeron and two reggeons) plus off-shell bare pion propagator depicted as dashed straight line. RB: the same as PB, but with the reggeized off-shell pion propagator depicted as dashed zigzag line. PF: central part of the diagram contains full eikonalized pion-proton amplitudes plus off-shell bare pion propagator depicted as dashed straight line. RF: the same as previous but with reggeized off-shell pion propagator depicted as dashed zigzag line. Proton-proton rescatterings in the initial and final states are depicted as V_{pp} and V'_{pp} -blobs correspondingly, and pion-proton rescattering corrections are also shown as $S_{\pi p}$ -blobs. For proton-proton and proton-pion elastic amplitudes we use the model of [21], [22] (see Appendix B). Off-shell pion form factor is presented as a black circle. Possible final pion-pion interaction is not shown, since we neglect it in the present calculations. But some authors [23] have proposed recently such a parametrization for low energy. RB and PB cases of Fig. 3 are similar to the one in Fig. 2.

1 General framework for calculations of LM CEDP

LM CEDP is the first exclusive two to four process which is driven by the Pomeron-Pomeron fusion subprocess. That is why it serves as a basic background for LM CEDP of resonances like $f_0(980)$, $f_2(1270)$. At the moment, for low central pion masses (less than ~ 3 GeV), it is a huge problem to use perturbative ap-

proach, that is why we apply the Regge-eikonal method for all the calculations. For proton-proton and proton-pion elastic amplitudes we use the model of [21], [22], which describe all the available experimental data on elastic scattering.

1.1 Components of the framework

LM CEDP process can be calculated in the following scheme (see Fig. 3):

1. We calculate the primary amplitude of the process, which is depicted as the central part of diagrams in Fig. 3. Here we consider four cases to show that only one of them gives the best description of the data on this process. The case PB represent the Born term (in each shoulder of the central primary amplitude), i.e. here we use the Born term for pion-proton elastic subamplitudes (see Appendix B) as other authors. Propagator for the off-shell pion is taken in its simple bare form $1/(\hat{t} - m_\pi^2)$. The case RB is similar to the previous one, but the bare off-shell pion propagator is replaced by the reggeized one

$$\mathcal{P}_\pi(\hat{s}, \hat{t}) = \left(\text{ctg} \frac{\pi \alpha_\pi(\hat{t})}{2} - i \right) \cdot \frac{\pi \alpha'_\pi}{2 \Gamma(1 + \alpha_\pi(\hat{t}))} \left(\frac{\hat{s}}{s_0} \right)^{\alpha_\pi(\hat{t})}, \quad (1)$$

where \hat{s} is the di-pion mass squared and \hat{t} is the square of the momentum transfer between a Pomeron and a pion in the Pomeron-Pomeron fusion process (see Appendix A for details).

The cases PF (RF) can be obtained from PB (RB) if we replace Born pion-proton elastic amplitudes to full eikonalized expressions, which could be found in Appendix B.

2. After the calculation of the primary LM CEDP amplitude we have to take into account all possible corrections in proton-proton and proton-pion elastic channels due to the unitarization procedure (so called “soft survival probability” or “rescattering corrections”), which are depicted as S_{pp} , S'_{pp} and $S_{\pi p}$ blobs in Fig. 3.

In this article we do not consider so called “enhanced” corrections [7]-[9], since they give nonleading contributions in our model due to smallness of the triple Pomeron vertex. Also we have no possible absorptive corrections in the pion-pion final elastic channel, since the central mass is low, and also there is a lack of data on this process to define parameters of the model. Nevertheless we will consider these corrections in further

works, as it was done by some authors recently [23], since they could play significant role for masses less than 1 GeV.

Exact kinematics of the two to four process is outlined in Appendix A.

Here we use the model, presented in Appendix B for example. You can use another one, which describe well all the available data on proton-proton and proton-pion elastic processes. It is difficult to find now more than a couple of models which have more or less predictable power (see [24] for detailed discussion). That is why we use the model, which is rather good in data fitting, especially in the kinematical region of our interest.

Final expression for the amplitude with proton-proton and pion-proton “rescattering” corrections can be written as

$$\begin{aligned} M^U(\{p\}) &= \\ &= \int \int \frac{d^2 \mathbf{q}}{(2\pi)^2} \frac{d^2 \mathbf{q}'}{(2\pi)^2} \frac{d^2 \mathbf{q}_1}{(2\pi)^2} \frac{d^2 \mathbf{q}_2}{(2\pi)^2} V_{pp}(s, q^2) V_{pp}(s', q'^2) \\ &\times [S_{\pi-p}(\tilde{s}_{14}, q_1^2) M_0(\{\tilde{p}\}) S_{\pi+p}(\tilde{s}_{23}, q_2^2) + (3 \leftrightarrow 4)] \quad (2) \\ M_0(\{p\}) &= \\ &= T_{\pi+p}^{el}(s_{13}, t_1) \mathcal{P}_\pi(\hat{s}, \hat{t}) \left[\hat{F}_\pi(\hat{t}) \right]^2 T_{\pi-p}^{el}(s_{24}, t_2), \quad (3) \end{aligned}$$

where sets of vectors are

$$\{p\} \equiv \{p_a, p_b, p_1, p_2, p_3, p_4\} \quad (4)$$

$$\begin{aligned} \{\tilde{p}\} &\equiv \{p_a - q, p_b + q; p_1 + q' + q_1, \\ &\quad p_2 - q' + q_2, p_3 - q_2, p_4 - q_1\}, \quad (5) \end{aligned}$$

and

$$\tilde{s}_{14} = (p_1 + p_4 + q')^2, \quad \tilde{s}_{23} = (p_2 + p_3 - q')^2, \quad (6)$$

$$s_{ij} = (p_i + p_j)^2, \quad t_{1,2} = (p_{a,b} - p_{1,2})^2, \quad (7)$$

$$\hat{s} = (p_3 + p_4)^2, \quad \hat{t} = (p_a - p_1 - p_3)^2 \quad (8)$$

Off-shell pion form factor is equal to unity on mass shell $\hat{t} = m_\pi^2$ and taken as exponential

$$\hat{F}_\pi = e^{(\hat{t} - m_\pi^2)/\Lambda_\pi^2}, \quad (9)$$

where Λ_π is taken from the fits to LM CEDP of two pions at low energies (see next section). In this paper we use only exponential form, but it is possible to use other parametrizations (see [7]-[12]). Exponential one shows more appropriate results in the data fitting.

Other functions are defined in Appendix B. Then we can use the expression (21) to calculate the differential cross-section of the process.

1.2 Nuances of calculations.

In the next section one can see that there are some difficulties in the data fitting, which have also been presented in other works [10]-[12]. In this subsection let

us discuss some nuances of calculations, which could change the situation.

We have to pay special attention to amplitudes, where one or more external particles are off their mass shell. The example of such an amplitude is the pion-proton one T_{π^+p} (T_{π^-p}), which is the part of the CEDP amplitude (see (2)). For this amplitude in the present paper we use Regge-eikonal model with the eikonal function in the classical Regge form. And “off-shell” condition for one of the pions is taken into account by additional phenomenological form factor $\hat{F}_\pi(\hat{t})$. But there are at least two other possibilities.

The first one was considered in [25]. For amplitude with one particle off-shell the formula

$$T^*(s, b) = \frac{\delta^*(s, b)}{\delta(s, b)} T(s, b) = \frac{\delta^*(s, b)}{\delta(s, b)} \frac{e^{2i\delta(s, b)} - 1}{2i} \quad (10)$$

was used. In our case

$$\begin{aligned} \delta(s, b) &= \delta_{\pi p}(s, b; m_\pi^2, m_\pi^2, m_p^2, m_p^2), \\ \delta^*(s, b) &= \delta_{\pi p}^*(s, b; \hat{t}, m_\pi^2, m_p^2, m_p^2) \\ \delta_{\pi p} &= \delta_{\pi p}^*|_{\hat{t} \rightarrow m_\pi^2}. \end{aligned} \quad (11)$$

This is similar to the introduction of the additional form factor, but in a more consistent way, which takes into account the unitarity condition.

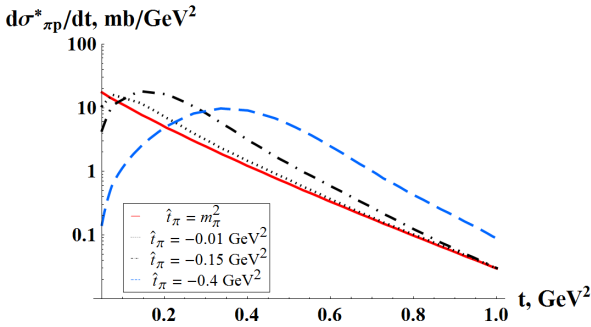


Fig. 4 Pion-proton on-shell and off-shell elastic differential cross-section (in the model of conserved meson currents presented in Appendix C) for different pion virtualities \hat{t}_π : m_π^2 (on-shell), -0.01 GeV^2 , -0.15 GeV^2 , -0.4 GeV^2 in the covariant approach with conserved currents (47).

The second one arises from the covariant reggeization method, which is considered in Appendix C. For the case of conserved hadronic currents we have definite structure in the Legendre function (47), which is transformed in a natural way to the case of the off-shell amplitude. But in this case off-shell amplitude has a specific behaviour at low t values (see Fig. 4 and [2] for details). As was shown in [2], unitarity corrections can

mask this behavior. To check this we need to make all the calculations and fitting of the data for the process $p + p \rightarrow p + \pi + \pi + p$, but with the amplitude like (47) instead of (31). This will be done in further works on the subject.

In the present calculations we use linear pion trajectory $0.7(\hat{t} - m_\pi^2)$. Nonlinear case was also verified, and the difference in the final result is not significant.

2 Data from hadron colliders versus results of calculations

Our basic task is to extract the fundamental information on the interaction of hadrons from different cross-sections (“diffractive patterns”):

- from t -distributions we can obtain size and shape of the interaction region;
- the distribution on the azimuthal angle between final protons gives quantum numbers of the produced system (see [2],[26] and references therein);
- from M_c (here $M_c = M_{\pi\pi}$) dependence and its influence on t -dependence we can make some conclusions about the interaction at different space-time scales and interrelation between them.

Process $p + p \rightarrow p + \pi + \pi + p$ is the first “standard candle”, which we can use to estimate other LM CEDP processes, like a resonance production [26],[27]. In this section we consider the experimental data on the process and its description for different model cases.

2.1 STAR collaboration data versus model cases

In this subsection the data of the STAR collaboration [15],[16] and model curves for different cases of Fig. 3 are presented. In our approach we have only one free parameter Λ_π , that is why all the distributions are depicted for its different values. Also in every case we consider two possibilities, with all rescattering corrections (two upper pictures) and with proton-proton rescattering only (i.e. without pion-proton interaction in the final state, two lower pictures). We change Λ_π and try to get the best description. As you can see from figures 5-8, the best description is given in the RF case with or without final pion-proton rescattering (see Fig. 5). Since final pion-proton interaction can give rather large suppression (about 10-20%, as in Fig. 14), in our further calculations we use the full amplitude as depicted in Fig. 3 for the RF case. The RF case without pion-proton interactions in the final state (with its own values of Λ_π for the best data description) we will show just for the check out of this possibility.

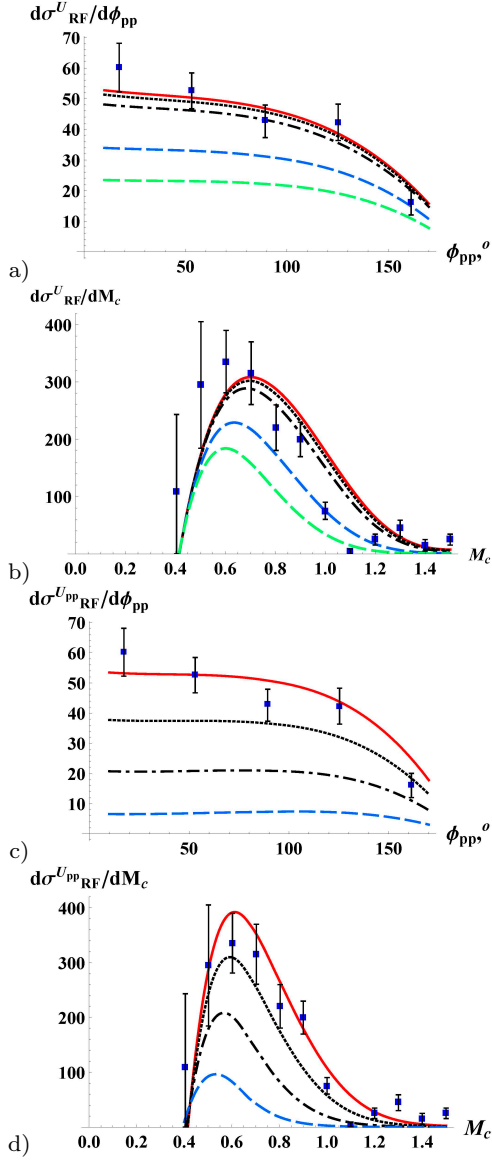


Fig. 5 RF case of the model (see Fig. 3). The data on the process $p + p \rightarrow p + \pi^+ + \pi^- + p$ at $\sqrt{s} = 200$ GeV, $|\eta_\pi| < 1$, $|\eta_{\pi\pi}| < 2$, $p_{T\pi} > 0.15$ GeV, $0.005 < -t_{1,2} < 0.03$ GeV², (STAR collaboration [15],[16]). Pictures (a), (b) show the result with all p p and π p rescattering corrections, pictures (c), (d) show the result without π p rescattering. Curves from up to down correspond to different values of the parameter Λ_π in the off-shell pion form factor (9): (a),(b) $\Lambda_\pi = 5, 4, 3, 1.6, 1.2$ GeV, (c),(d) $\Lambda_\pi = 1.2, 1, 0.8, 0.6$ GeV.

2.2 ISR and CDF data versus RF case of the model

Let us look at the ISR [13],[14] and CDF [17],[18] data with parameter Λ_π , which we use to describe the data from STAR collaboration. Different cases are depicted on Figs. 9-12.

We see underestimation of the ISR data. For these low energies we have to take into account possible cor-

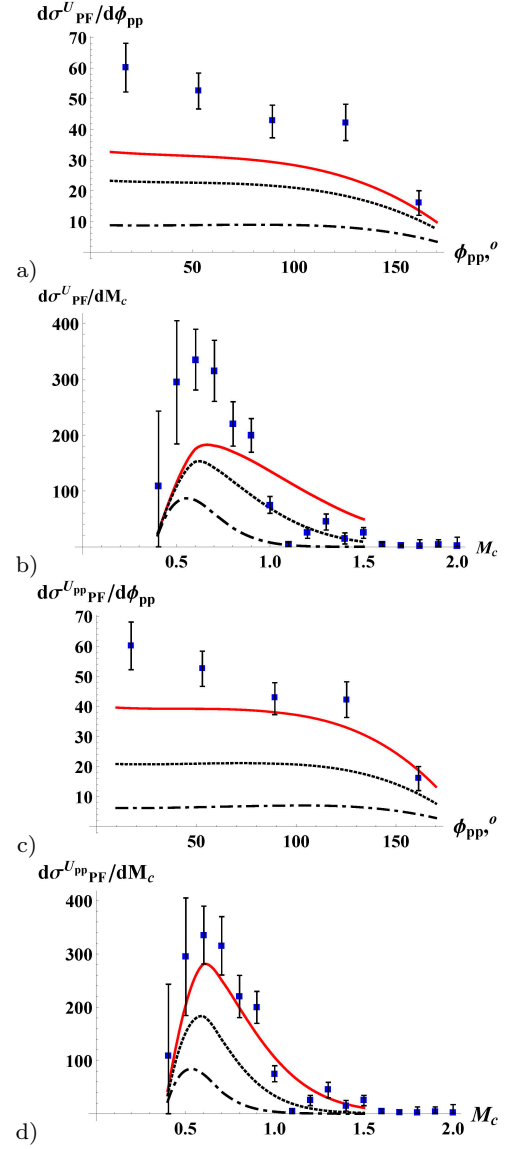


Fig. 6 PF case of the model (see Fig. 3). The data on the process $p + p \rightarrow p + \pi^+ + \pi^- + p$ at $\sqrt{s} = 200$ GeV, $|\eta_\pi| < 1$, $|\eta_{\pi\pi}| < 2$, $p_{T\pi} > 0.15$ GeV, $0.005 < -t_{1,2} < 0.03$ GeV², (STAR collaboration [15],[16]). Pictures (a), (b) show the result with all p p and π p rescattering corrections, pictures (c), (d) show the result without π p rescattering. Curves from up to down correspond to different values of the parameter Λ_π in the off-shell pion form factor (9): (a),(b) $\Lambda_\pi = 1.6, 1.2, 0.8$ GeV, (c),(d) $\Lambda_\pi = 1, 0.8, 0.6$ GeV.

rections to pion-proton amplitudes, since our approach describe data well only for energies greater than ~ 3 GeV. And in each shoulder ($T_{\pi p}$ amplitude in Fig. 3 RF) energy can be less than 3 GeV.

As to the CDF data (Figs. 11, 12), which is overestimated for $M_{\pi\pi} < 1.5$ GeV, we can say that measurements were done only with one final hadron detected, that is why there are possible contributions of dissociation to the data. Also there are corrections (destructive

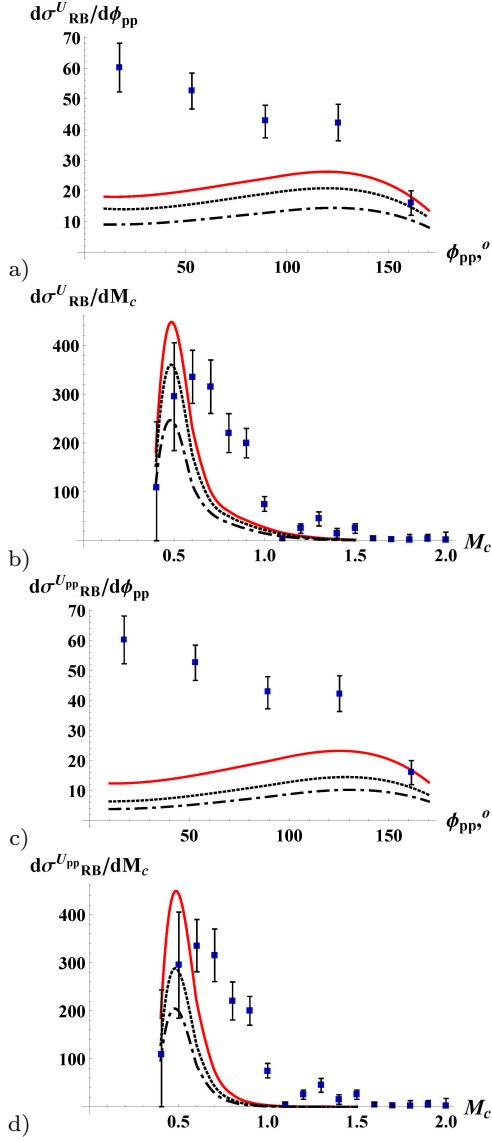


Fig. 7 RB case of the model (see Fig. 3). The data on the process $p + p \rightarrow p + \pi^+ + \pi^- + p$ at $\sqrt{s} = 200$ GeV, $|\eta_\pi| < 1$, $|\eta_{\pi\pi}| < 2$, $p_{T\pi} > 0.15$ GeV, $0.005 < -t_{1,2} < 0.03$ GeV², (STAR collaboration [15],[16]). Pictures (a),(b) show the result with all p p and π p rescattering corrections, pictures (c), (d) show the result without π p rescattering. Curves from up to down correspond to different values of the parameter Λ_π in the off-shell pion form factor (9): (a),(b) $\Lambda_\pi = 0.45, 0.43, 0.4$ GeV, (c),(d) $\Lambda_\pi = 0.4, 0.37, 0.35$ GeV.

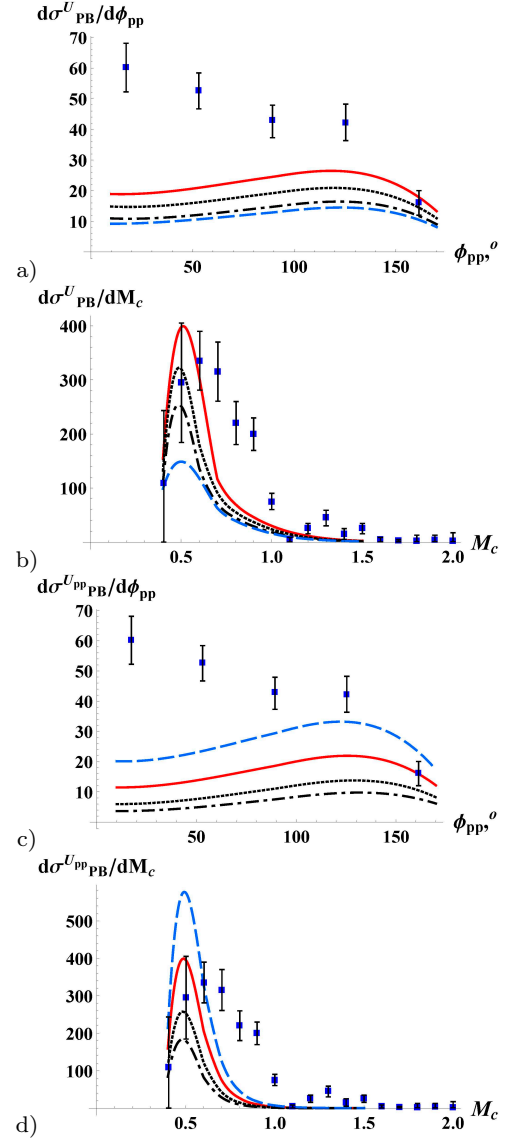


Fig. 8 PB case of the model (see Fig. 3). The data on the process $p + p \rightarrow p + \pi^+ + \pi^- + p$ at $\sqrt{s} = 200$ GeV, $|\eta_\pi| < 1$, $|\eta_{\pi\pi}| < 2$, $p_{T\pi} > 0.15$ GeV, $0.005 < -t_{1,2} < 0.03$ GeV², (STAR collaboration [15],[16]). Pictures (a),(b) show the result with all p p and π p rescattering corrections, pictures (c), (d) show the result without π p rescattering. Curves from up to down correspond to different values of the parameter Λ_π in the off-shell pion form factor (9): (a),(b) $\Lambda_\pi = 0.45, 0.43, 0.41, 0.4$ GeV, (c),(d) $\Lambda_\pi = 0.43, 0.4, 0.37, 0.35$ GeV.

interference terms) from resonances to the amplitude, like in Fig. 3 of [10],[11] and other effects for low $M_{\pi\pi}$, for example, the interference with $\gamma\gamma$ or $\gamma\mathbb{O}$ fusion in the central production process.

2.3 CMS data and predictions

In Fig. 13 one can see the recent data from the CMS collaboration and curves of our model. Upper curve, that corresponds to the parameter Λ_π , which better fits the STAR data on ϕ_{pp} distribution (but gives higher values for $M_{\pi\pi} > 1$ GeV as depicted in Fig. 5b), also describes the data of CMS collaboration well (but overestimates

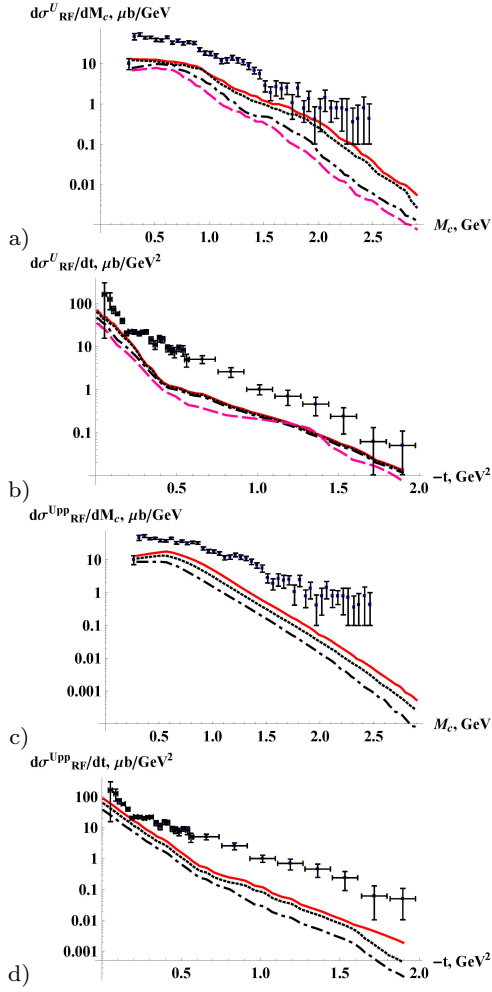


Fig. 9 RF case of the model (see Fig. 3) with all rescattering corrections (a, b) and without final pion-proton rescattering (c, d). The data on the process $p + p \rightarrow p + \pi^+ + \pi^- + p$ at $\sqrt{s} = 63$ GeV, $|y_\pi| < 1$, $\xi_p > 0.9$, (ISR and ABCDHW collaborations [13],[14]). Curves from up to down correspond to different values of the parameter Λ_π in the off-shell pion form factor (9): (a),(b) $\Lambda_\pi = 4, 3, 1.6, 1.2$ GeV, (c),(d) $\Lambda_\pi = 1.2, 1, 0.8$ GeV.

the CDF data, as was shown in Figs. 11, 12). Lower curve underestimates the data from STAR, ISR and CMS, but is close to the CDF data. Interference with resonance contributions change the picture, especially for low $M_{\pi\pi}$, that is why we have to take it into account when fitting the data.

2.4 Summary

After the experimental data analysis we have several facts:

- in our approach the best description is given by the case RF (Fig. 3). That is why effects from rescattering (unitarity) corrections are very important;

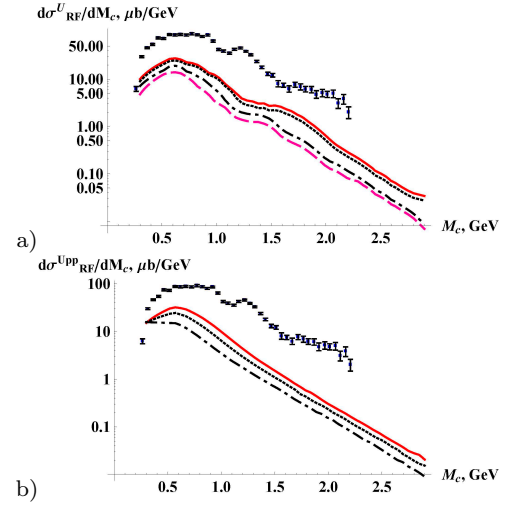


Fig. 10 RF case of the model (see Fig. 3) with all rescattering corrections (a) and without final pion-proton rescattering (b). The data on the process $p + p \rightarrow p + \pi^+ + \pi^- + p$ at $\sqrt{s} = 62$ GeV, $|y_\pi| < 1.5$, $\xi_p > 0.9$, (ISR and ABCDHW collaborations [13],[14]). Curves from up to down correspond to different values of the parameter Λ_π in the off-shell pion form factor (9): (a) $\Lambda_\pi = 4, 3, 1.6, 1.2$ GeV, (b) $\Lambda_\pi = 1.2, 1, 0.8$ GeV.

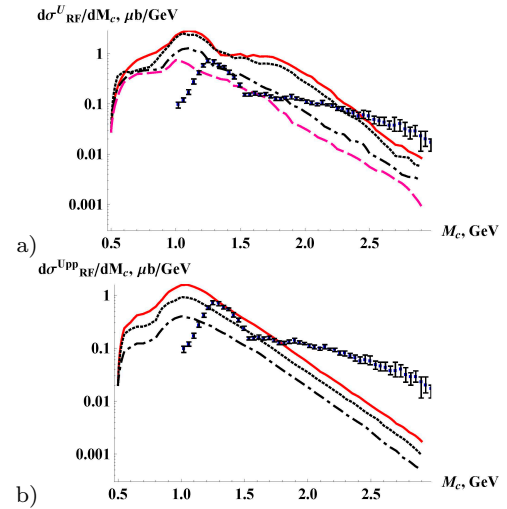


Fig. 11 RF case of the model (see Fig. 3) with all rescattering corrections (a) and without final pion-proton rescattering (b). The data on the process $p + \bar{p} \rightarrow p + \pi^+ + \pi^- + \bar{p}$ at $\sqrt{s} = 1.96$ TeV, $|\eta_\pi| < 1.3$, $|y_{\pi\pi}| < 1$, $p_{T,\pi} > 0.4$ GeV, (CDF collaboration [17],[18]). Curves from up to down correspond to different values of the parameter Λ_π in the off-shell pion form factor (9): (a) $\Lambda_\pi = 4, 3, 1.6, 1.2$ GeV, (b) $\Lambda_\pi = 1.2, 1, 0.8$ GeV.

- the result is crucially dependent on the choice of Λ_π in the off-shell pion form factor, i.e. on \hat{t} (virtuality of the pion) dependence;
- if we try to fit the data from STAR [15],[16], we find that the best description gives overestimation of the CDF data [17],[18] (especially in the region

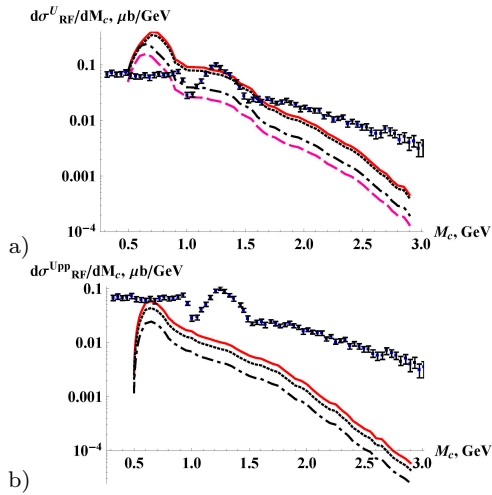


Fig. 12 RF case of the model (see Fig. 3) with all rescattering corrections (a) and without final pion-proton rescattering (b). The data on the process $p + \bar{p} \rightarrow p + \pi^+ + \pi^- + \bar{p}$ at $\sqrt{s} = 1.96$ TeV, $|\eta_\pi| < 1.3$, $|y_{\pi\pi}| < 1$, $p_{T,\pi} > 0.4$ GeV, $p_{T,\pi\pi} > 1$ GeV, (CDF collaboration [17],[18]). Curves from up to down correspond to different values of the parameter Λ_π in the off-shell pion form factor (9): (a) $\Lambda_\pi = 4, 3, 1.6, 1.2$ GeV, (b) $\Lambda_\pi = 1.2, 1, 0.8$ GeV.

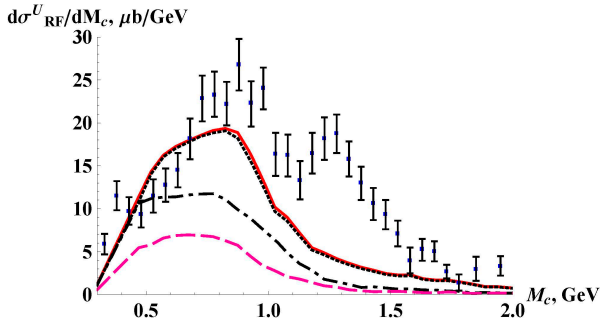


Fig. 13 RF case of the model (see Fig. 3) with all rescattering corrections. The data on the process $p + \bar{p} \rightarrow p + \pi^+ + \pi^- + \bar{p}$ at $\sqrt{s} = 7$ TeV, $|y_\pi| < 2$, $p_{T,\pi} > 0.2$ GeV, (CMS collaboration [19],[20]). Curves from up to down correspond to different values of the parameter Λ_π in the off-shell pion form factor (9): $\Lambda_\pi = 4, 3, 1.6, 1.2$ GeV.

$M_{\pi\pi} < 1.5$ GeV) and underestimation of the ISR data [13],[14]. This is due to effects like the interference with resonance contributions or $\gamma\gamma \rightarrow \pi\pi$ and $\gamma\mathbb{O} \rightarrow \pi\pi$ processes, corrections to pion-pion scattering at low $M_{\pi\pi}$, additional contributions of dissociation process to the CDF data, corrections to $T_{\pi p}(s, t)$ for $\sqrt{s} < 3$ GeV;

- predictions for CMS are close to the data, if we use the best fit to the STAR data on ϕ_{pp} distribution (see Fig.5b). We need also an estimate of the interference with resonance terms to see the full picture and make final conclusions.

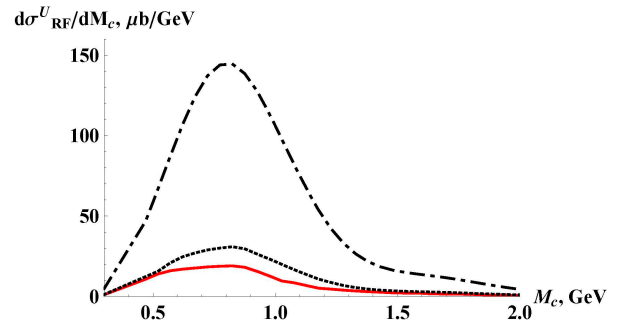


Fig. 14 RF case of the model (see Fig. 3) for the CMS energy. Curves from up to down correspond to the Born term, the amplitude with proton-proton rescattering corrections only and the one with all the corrections (proton-proton and pion-proton).

3 Pomeron-Pomeron to pion-pion cross-section

Another interesting question, which we can discuss here, concerns the Pomeron-Pomeron cross-section. As was shown in [3], it is possible to extract the Pomeron-proton cross-section from the data on single (SD) and double (DD) dissociation, and this numerical value occurs to be of the order of typical hadron-hadron cross-sections. It was done by the use of covariant reggeization method with conserved spin-J meson currents, which helps to solve the old problem of very small Pomeron-proton cross-section extracted by other authors [28]-[29].

Reggeon-hadron and reggeon-reggeon scattering can be considered as a scattering of all possible real mesons lying on the Regge trajectory of hadrons. Conceptually it is similar to Hydrogen-hadron or Hydrogen-Hydrogen scattering, since Hydrogen has the spectrum of states, and each of them has its own probability to scatter on a hadron or another hydrogen atom. Specific feature is that we deal in this case with “off-shell atoms”.

As was shown also in [3], absorptive corrections play the crucial role in high energy scattering, and make the extraction procedure rather complicated and model dependent. We should propose some appropriate parametrization for Pomeron-hadron cross-section, then we apply unitarization procedure to obtain real SD or DD cross-sections.

It is possible to perform a similar procedure to extract Pomeron-Pomeron cross-section. In further works we shall consider the extraction of the total Pomeron-Pomeron cross-section. Here we restrict ourselves by the extraction of the Pomeron-Pomeron to pion-pion one. Let us use the parametrization (2) for CEDP di-pion production to fix one parameter Λ_π from the experimental data. After that we can simply estimate Pomeron-Pomeron to di-pion cross-section (we use the

covariant method from Appendix C):

$$\begin{aligned}
& \frac{d\sigma_{J_1 J_2 \rightarrow \pi\pi}(\hat{s})}{d\hat{t}} = \\
& \frac{1}{(2J_1+1)(2J_2+1)} \frac{1}{16\pi\lambda(\hat{s}, t_1, t_2)} \left| \mathcal{P}_\pi(\hat{s}, \hat{t}) \hat{F}_\pi(\hat{t})^2 \right| \times \\
& \sum_{\lambda_1, \lambda_2} \left| e_{\mu_1 \dots \mu_{J_1}}^{(\lambda_1)}(t_1) e_{\nu_1 \dots \nu_{J_2}}^{(\lambda_2)}(t_2) F_{\mu_1 \dots \mu_{J_1}, \nu_1 \dots \nu_{J_2}}^{J_1 J_2 \rightarrow \pi\pi} \right|^2 = \\
& \frac{1}{(2J_1+1)(2J_2+1)} \frac{1}{16\pi\lambda(\hat{s}, t_1, t_2)} \left| \mathcal{P}_\pi(\hat{s}, \hat{t}) \hat{F}_\pi(\hat{t})^2 \right| \times \\
& \Pi_{\mu_1 \dots \mu_{J_1}}^{\mu'_1 \dots \mu'_{J_1}}(t_1) \Pi_{\nu_1 \dots \nu_{J_2}}^{\nu'_1 \dots \nu'_{J_2}}(t_2) W_{\mu'_1 \dots \mu'_{J_1}, \nu'_1 \dots \nu'_{J_2}}^{\mu_1 \dots \mu_{J_1}, \nu_1 \dots \nu_{J_2}} = \\
& \frac{\left| \mathcal{P}_\pi(\hat{s}, \hat{t}) \hat{F}_\pi(\hat{t})^2 g_{J_1}^\pi(t_1) g_{J_2}^\pi(t_2) \right|^2 \prod_{i=1}^2 \frac{2^{J_i-1} (J_i-1)! J_i!}{(2J_i-1)!}}{(2J_1+1)(2J_2+1) \cdot 16\pi\lambda(\hat{s}, t_1, t_2)} \times \\
& \times \mathcal{F}_{J_1}(t_1, \hat{t}) \mathcal{F}_{J_2}(t_2, \hat{t}) \quad (12)
\end{aligned}$$

Here $\Pi_{\mu_1 \dots \mu_{J_i}}^{\mu'_1 \dots \mu'_{J_i}} = \sum_\lambda e_{\mu'_1 \dots \mu'_{J_i}}^{(\lambda)} e_{\mu_1 \dots \mu_{J_i}}^{*(\lambda)}$ is the structure in the propagator like (50), $e_{\mu_1 \dots \mu_{J_i}}^{(\lambda)}$ are polarization tensors, $F_{\mu_1 \dots \mu_{J_1}, \nu_1 \dots \nu_{J_2}}^{J_1 J_2 \rightarrow \pi\pi}$ is the Pomeron-Pomeron amplitude and $W_{\mu'_1 \dots \mu'_{J_1}, \nu'_1 \dots \nu'_{J_2}}^{\mu_1 \dots \mu_{J_1}, \nu_1 \dots \nu_{J_2}}$ is the hadronic tensor for this process made of Pomeron-pion-pion vertexes $T_{\mu_1 \dots \mu_{J_i}}(p, \Delta)$, where $g_J^\pi(t) = F_J(t)/(m_\pi^2 - t/4)^{J/2}$, F_J is the leading form factor from (43). After reggeization we get

$$\begin{aligned}
& \frac{d\sigma_{\mathbb{P}\mathbb{P} \rightarrow \pi\pi}(\hat{s})}{d\hat{t}} = \prod_{i=1}^2 \frac{2^{\alpha_{\mathbb{P}}(t_i)-1} \Gamma(\alpha_{\mathbb{P}}(t_i)) \Gamma(\alpha_{\mathbb{P}}(t_i) + 1)}{\Gamma(2\alpha_{\mathbb{P}}(t_i))} \\
& \frac{\left| \mathcal{P}_\pi(\hat{s}, \hat{t}) \hat{F}_\pi(\hat{t})^2 g^\pi(t_1) g^\pi(t_2) \right|^2 \mathcal{F}(t_1, \hat{t}) \mathcal{F}(t_2, \hat{t})}{(2\alpha_{\mathbb{P}}(t_1) + 1)(2\alpha_{\mathbb{P}}(t_2) + 1) \cdot 16\pi\lambda(\hat{s}, t_1, t_2)}, \quad (13)
\end{aligned}$$

$$g^\pi(t) = \frac{\beta_{\mathbb{P}}(t) 2^{\alpha_{\mathbb{P}}(t)}}{\pi \alpha'_{\mathbb{P}}(t) g^p(t)}, \quad (14)$$

where all the functions are defined in Appendix B. If we use approach (14), where all terms like

$$2\sqrt{-t} \lambda^{1/2}(m_i^2, m_j^2, t)$$

in (47) are absorbed to the residue, we have to multiply the result by the additional factor $\mathcal{F}(t_1, \hat{t}) \mathcal{F}(t_2, \hat{t})$, where

$$\mathcal{F}(t, \hat{t}) = \left(\frac{m_\pi^2 - \frac{(m_\pi^2 - \hat{t} + t)^2}{4t}}{s_0} \right)^{\alpha_{\mathbb{P}}(t)} \quad (15)$$

for conserved currents, and

$$\mathcal{F}(t, \hat{t}) \simeq \left(\frac{m_\pi^2 - \frac{(m_\pi^2 - \hat{t} + t)^2}{4m_J^2}}{s_0} \right)^{\alpha_{\mathbb{P}}(t)} \quad (16)$$

is the leading term for the case of nonconserved currents (see (50)).

Results of calculations (13)-(16) are shown in Fig. 15.

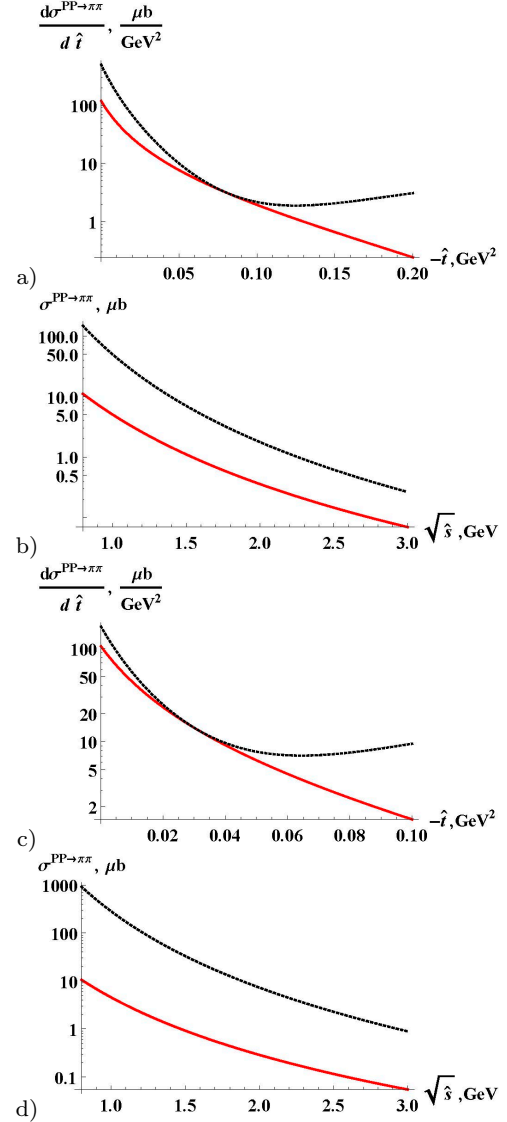


Fig. 15 Results of calculations (13)-(15) for Pomeron-Pomeron to pion-pion cross-section for $t_{1,2} = -0.1 \text{ GeV}^2$ (a,b) and $t_{1,2} = -0.05 \text{ GeV}^2$ (c,d). Two curves present cases of nonconserved (solid) and conserved (dotted) hadronic currents. $\sqrt{\hat{s}} = 1.5 \text{ GeV}$ in (a), (c). The parameter of the off-shell form factor is taken $\Lambda_\pi = 1 \text{ GeV}$.

In the old works [30]-[34] extracted Pomeron-Pomeron total cross-section is of the order $100 \mu b$ and almost independent on Pomeron's virtuality at $\sqrt{\hat{s}} < 3 \text{ GeV}$. $\sigma_{\mathbb{P}\mathbb{P} \rightarrow \pi\pi}$ should be at least less than this number. Our calculations in the same kinematical region give numbers of the order $0.1 \rightarrow 1 \mu b$. This low value shows the role of other processes (especially production of resonances) in this region, where resonances give the main contribution to $\sigma_{\mathbb{P}\mathbb{P}}^{\text{tot}}$.

In section 2 it is shown that only RF mode (see Fig. 3 for notations) gives appropriate description of the data, i. e. we have to take into account all rescat-

tering corrections even in the $T_{\pi p}$ amplitudes. If to use RB mode, as some other authors do [7]-[12], it is possible to extract the Pomeron-Pomeron cross-section easier (“almost model independent method”, as was done, for example, for the pion-proton cross-section [35]).

Conclusions

In this paper we have considered the process LM CEDP of di-pions and its description in the framework of the Regge-eikonal approach. Here we summarize all the facts and conclusions:

- after calculations of several cases (see Fig. 3) we can see that RF case is more appropriate to describe the data on the process $p + p \rightarrow p + \pi^+ + \pi^- + p$.
- when we try to fit the data from STAR collaboration [15],[16] with different values of Λ_π (different behavior of the virtual pion form factor), we obtain underestimation of the ISR data [13],[14] and overestimation of the CDF [17],[18]. Possible explanations are: interference terms with resonances, possible corrections to $T_{\pi p}(s, t)$ for $\sqrt{s} < 3$ GeV, off-shell pion effects, some other mechanisms in Pomeron-Pomeron to pion-pion process at low $M_{\pi\pi}$, contributions from dissociative processes (in CDF or CMS data).
- we have rather good predictions to the CMS data, when we use the fit to STAR data on ϕ_{pp} distribution depicted on Fig. 5b, but we have to take into account interference with resonances to see the full picture. These main open problems regarding model parameters are related to interference terms (we have to know all couplings of pions to resonances), which require full spectrum simulation comparisons with data simultaneously in several differential observables. It should be done in further works.
- after estimations of the Pomeron-Pomeron to pion-pion cross-section in the framework of covariant reggeization approach we obtain cross-sections which are much lower ($\sim 0.1 \div 1 \mu b$) than the total Pomeron-Pomeron cross-section, estimated by other authors ($\sim 100 - 300 \mu b$), which shows possible contributions from other processes (especially from resonance production).

In further works we will take into account possible modifications of the model (amplitudes for resonances in LM CEDP and their interference with di-pion one, pion-pion cross-section, additional off-shell effects in subamplitudes and so on) for best description of the data. This model will be implemented to the Monte-carlo event generator ExDiff [36]. It is possible to cal-

culate LM CEDP for other di-hadron final states ($p\bar{p}$ for “Odderon” hunting, K^+K^- , $\eta\eta'$ and so on), which are also very informative for our understanding of diffractive mechanisms in strong interactions.

Acknowledgements

I am grateful to Vladimir Petrov and Anton Godizov for useful discussions.

Appendix A. Kinematics of LM CEDP

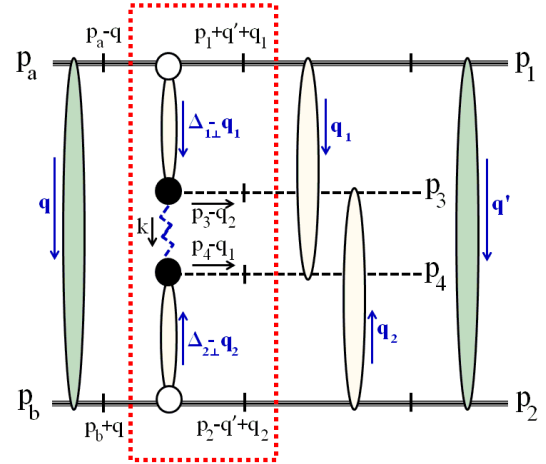


Fig. 16 Total amplitude of the process of double pion LM CEDP $p + p \rightarrow p + \pi^+ + \pi^- + p$ with detailed kinematics. Proton-proton rescatterings in the initial and final states are depicted as black blobs, and pion-proton subamplitudes are also shown as shaded blobs. All momenta are shown. Basic part of the amplitude, M_0 (see eq. (3)), without corrections is circled by a dotted line. Crossed lines are on mass shell. Here $\Delta_{1\perp} = \Delta_1 - q - q'$, $\Delta_{2\perp} = \Delta_2 + q + q'$, $\hat{t} = k^2 = (\Delta_{1\perp} - q_1 - p_3 + q_2)^2$, $\hat{u} = (\Delta_{1\perp} - q_1 - p_4)^2$, $\hat{s} = (p_3 + p_4 - q_1 - q_2)^2$.

The $2 \rightarrow 4$ process $p(p_a) + p(p_b) \rightarrow p(p_1) + \pi(p_3) + \pi(p_4) + p(p_2)$ can be described as follows (the notation

for any momentum is $k = (k_0, k_z; \mathbf{k})$, $\mathbf{k} = (k_x, k_y)$:

$$\begin{aligned} p_a &= \left(\frac{\sqrt{s}}{2}, \beta \frac{\sqrt{s}}{2}; \mathbf{0} \right), \quad p_b = \left(\frac{\sqrt{s}}{2}, -\beta \frac{\sqrt{s}}{2}; \mathbf{0} \right), \\ p_{1,2} &= (E_{1,2}, p_{1,2z}; \mathbf{p}_{1,2\perp}), \quad E_{1,2} = \sqrt{p_{1,2z}^2 + \mathbf{p}_{1,2\perp}^2 + m_p^2}, \\ p_{3,4} &= (m_{3,4\perp} \text{ch } y_{3,4}, m_{3,4\perp} \text{sh } y_{3,4}; \mathbf{p}_{3,4\perp}) = \\ &= \left(\sqrt{m_\pi^2 + \mathbf{p}_{3,4\perp}^2} \text{ch } \eta_{3,4}, |\mathbf{p}_{3,4\perp}| \text{sh } \eta_{3,4}; \mathbf{p}_{3,4\perp} \right), \\ m_{i\perp}^2 &= m_i^2 + \mathbf{p}_{i\perp}^2, \quad m_{1,2} = m_p, \quad m_{3,4} = m_\pi, \\ \mathbf{p}_{4\perp} &= -\mathbf{p}_{3\perp} - \mathbf{p}_{1\perp} - \mathbf{p}_{2\perp}, \\ \beta &= \sqrt{1 - \frac{4m_p^2}{s}}, \quad s = (p_a + p_b)^2, \quad s' = (p_1 + p_2)^2. \end{aligned} \quad (17)$$

Here y_i (η_i) are rapidities (pseudorapidities) of final pions.

Phase space of the process in terms of the above variables is the following

$$\begin{aligned} d\Phi_{2 \rightarrow 4} &= (2\pi)^4 \delta^4 \left(p_a + p_b - \sum_{i=1}^4 p_i \right) \prod_{i=1}^4 \frac{d^3 p_i}{(2\pi)^3 2E_i} = \\ &= \frac{1}{2^4 (2\pi)^8} \prod_{i=1}^3 p_{i\perp} dp_{i\perp} d\phi_i \cdot dy_3 dy_4 \cdot \mathcal{J}; \\ \mathcal{J} &= \frac{dp_{1z}}{E_1} \frac{dp_{2z}}{E_2} \delta \left(\sqrt{s} - \sum_{i=1}^4 E_i \right) \delta \left(\sum_{i=1}^4 p_{iz} \right) = \\ &= \frac{1}{|\tilde{E}_2 \tilde{p}_{1z} - \tilde{E}_1 \tilde{p}_{2z}|}, \end{aligned} \quad (18)$$

where $p_{i\perp} = |\mathbf{p}_i|$, $\tilde{p}_{1,2z}$ are appropriate roots of the system

$$\begin{cases} A = \sqrt{s} - E_3 - E_4 = \sqrt{m_{1\perp}^2 + p_{1z}^2} + \sqrt{m_{2\perp}^2 + p_{2z}^2}, \\ B = -p_{3z} - p_{4z} = p_{1z} + p_{2z}, \end{cases} \quad (19)$$

$$\begin{aligned} \tilde{p}_{1z} &= \frac{B}{2} + \frac{1}{2(A^2 - B^2)} \left[B(m_{1\perp}^2 - m_{2\perp}^2) + A \cdot \lambda_0^{1/2} \right], \\ \lambda_0 &= \lambda(A^2 - B^2, m_{1\perp}^2, m_{2\perp}^2). \end{aligned} \quad (20)$$

Here $\lambda(x, y, z) = x^2 + y^2 + z^2 - 2xy - 2xz - 2yz$, and then $\mathcal{J} = \lambda_0^{1/2}/2$.

For the differential cross-section we have

$$\begin{aligned} \frac{d\sigma_{2 \rightarrow 4}}{\prod_{i=1}^3 dp_{i\perp} d\phi_i \cdot dy_3 dy_4} &= \frac{1}{2\beta s} \cdot \frac{\prod_{i=1}^3 p_{i\perp}}{2^4 (2\pi)^8 \cdot \frac{1}{2} \lambda_0^{1/2}} |T|^2 = \\ &= \frac{\prod_{i=1}^3 p_{i\perp}}{2^{12} \pi^8 \beta s \lambda_0^{1/2}} |T|^2. \end{aligned} \quad (21)$$

Pseudorapidity is more convenient experimental variable, and we can use the transform

$$\frac{dy_i}{d\eta_i} = \frac{p_{i\perp} \text{ch } \eta_i}{\sqrt{m_i^2 + p_{i\perp}^2} \text{ch } \eta_i} \quad (22)$$

to get the differential cross-section in pseudorapidities.

For exact calculations of elastic subprocesses (see Fig. 16) of the type $a(p_1) + b(p_2) \rightarrow c(p_1 - q_{el}) + d(p_2 + q_{el})$:

$$\begin{aligned} q_{el} &= (q_0, q_z; \mathbf{q}), \\ q_z &= -\frac{b}{2a} \left(1 - \sqrt{1 - \frac{4ac}{b^2}} \right), \\ q_0 &= \frac{A_0 q_z + \mathbf{p}_{1\perp} \mathbf{q} + \mathbf{p}_{2\perp} \mathbf{q}}{A_z}, \\ a &= A_z^2 - A_0^2, \quad b = -2(A_z \cdot \mathcal{D} + A_0(\mathbf{p}_{1\perp} \mathbf{q} + \mathbf{p}_{2\perp} \mathbf{q})), \\ c &= 2A_z B_z - (\mathbf{p}_{1\perp} \mathbf{q} + \mathbf{p}_{2\perp} \mathbf{q})^2 + \mathbf{q}^2 A_z^2, \\ A_0 &= p_{1z} + p_{2z}, \quad A_z = p_{10} + p_{20}, \\ B_0 &= p_{1z} \cdot \mathbf{p}_{2\perp} \mathbf{q} - p_{2z} \cdot \mathbf{p}_{1\perp} \mathbf{q}, \\ B_z &= p_{10} \cdot \mathbf{p}_{2\perp} \mathbf{q} - p_{20} \cdot \mathbf{p}_{1\perp} \mathbf{q}, \\ \mathcal{D} &= p_{1z} p_{20} - p_{2z} p_{10}, \end{aligned} \quad (23)$$

and $q_{el}^2 \simeq -\mathbf{q}^2$.

Appendix B. Regge-eikonal model for elastic proton-proton and pion-proton scattering

Here is a short review of formulae for the Regge-eikonal approach [21], [22], which we use to estimate rescattering corrections in the proton proton and pion proton channels.

Amplitudes of elastic proton-proton and pion-proton scattering are expressed in terms of eikonal functions

$$\begin{aligned} T_{pp, \pi p}^{el}(s, b) &= \frac{e^{-2\Omega_{pp, \pi p}^{el}(s, b)} - 1}{2i}, \\ \Omega_{pp, \pi p}^{el}(s, b) &= -i \delta_{pp, \pi p}^{el}(s, b), \\ \delta_{pp, \pi p}^{el}(s, b) &= \frac{1}{16\pi s} \int_0^\infty d(-t) J_0(b\sqrt{-t}) \delta_{pp, \pi p}^{el}(s, t). \end{aligned} \quad (24)$$

$$\begin{aligned} \delta_{pp}^{el}(s, t) &\simeq \\ g_{pp\mathbb{P}}(t)^2 \left(i + \tan \frac{\pi(\alpha_{\mathbb{P}}(t) - 1)}{2} \right) \pi \alpha'_{\mathbb{P}}(t) \left(\frac{s}{2s_0} \right)^{\alpha_{\mathbb{P}}(t)}, \\ \alpha_{\mathbb{P}}(t) &= 1 + \frac{\alpha_{\mathbb{P}}(0) - 1}{1 - \frac{t}{\tau_a}}, \quad g_{pp\mathbb{P}}(t) = \frac{g_{pp\mathbb{P}}(0)}{(1 - a_g t)^2}. \end{aligned} \quad (25)$$

$$\begin{aligned} \delta_{\pi p}^{el}(s, t) &\simeq \\ \left(i + \tan \frac{\pi(\alpha_{\mathbb{P}}(t) - 1)}{2} \right) \beta_{\mathbb{P}}(t) \left(\frac{s}{s_0} \right)^{\alpha_{\mathbb{P}}(t)}, \\ + \left(i + \tan \frac{\pi(\alpha_f(t) - 1)}{2} \right) \beta_f(t) \left(\frac{s}{s_0} \right)^{\alpha_f(t)}, \end{aligned} \quad (26)$$

$$\begin{aligned}
\alpha_{\mathbb{P}}(t) &= 1 + p_1 \left[1 - p_2 t \left(\arctan(p_3 - p_2 t) - \frac{\pi}{2} \right) \right], \\
\alpha_f(t) &= \left(\frac{8}{3\pi} \gamma(\sqrt{-t + c_f}) \right)^{1/2}, \\
\gamma(\mu) &= \frac{4\pi}{11 - \frac{2}{3}n_f} \left(\frac{1}{\ln \frac{\mu^2}{\Lambda^2}} + \frac{1}{1 - \frac{\mu^2}{\Lambda^2}} \right), \\
\beta_{\mathbb{P}}(t) &= B_{\mathbb{P}} e^{b_{\mathbb{P}} t} (1 + d_1 t + d_2 t^2 + d_3 t^3 + d_4 t^4), \\
\beta_f(t) &= B_f e^{b_f t}.
\end{aligned} \tag{27}$$

Parameters can be found in tables 1 and 2.

Table 1 Parameters for proton-proton elastic scattering amplitude.

Parameter	Value
$\alpha_{\mathbb{P}}(0) - 1$	0.109
τ_a	0.535 GeV ²
$g_{p p \mathbb{P}}(0)$	13.8 GeV
a_g	0.23 GeV ⁻²

Table 2 Parameters for pion-proton elastic scattering amplitude.

Parameter	Value
$B_{\mathbb{P}}$	26.7
$b_{\mathbb{P}}$	2.36 GeV ⁻²
d_1	0.38 GeV ⁻²
d_2	0.3 GeV ⁻⁴
d_3	-0.078 GeV ⁻⁶
d_4	0.04 GeV ⁻⁸
B_f	67
b_f	1.88 GeV ⁻²

$$\begin{aligned}
V_{pp}(s, q^2) &= \int d^2 \mathbf{b} e^{i \mathbf{q} \mathbf{b}} \sqrt{1 + 2i T_{pp}^{el}(s, b)} = \\
&= \int d^2 \mathbf{b} e^{i \mathbf{q} \mathbf{b}} e^{-\Omega_{pp}^{el}(s, b)} = \\
&= (2\pi)^2 \delta^2(\mathbf{q}) + 2\pi \bar{T}_{pp}(s, q^2),
\end{aligned} \tag{28}$$

$$\bar{T}_{pp}(s, q^2) = \int_0^\infty b db J_0(b\sqrt{-q^2}) \left[e^{-\Omega_{pp}^{el}(s, b)} - 1 \right] \tag{29}$$

$$\begin{aligned}
S_{\pi p}(s, q^2) &= \int d^2 \mathbf{b} e^{i \mathbf{q} \mathbf{b}} (1 + 2i T_{\pi p}^{el}(s, b)) = \\
&= \int d^2 \mathbf{b} e^{i \mathbf{q} \mathbf{b}} e^{-2\Omega_{\pi p}^{el}(s, b)} = \\
&= (2\pi)^2 \delta^2(\mathbf{q}) + 2\pi \bar{T}_{\pi p}(s, q^2),
\end{aligned} \tag{30}$$

$$\bar{T}_{\pi p}(s, q^2) = \int_0^\infty b db J_0(b\sqrt{-q^2}) \left[e^{-2\Omega_{\pi p}^{el}(s, b)} - 1 \right] \tag{31}$$

Approach (26) describes the data on pion-proton scattering better even at low energies, that is why we use it instead of the one presented in [21].

Functions \bar{T}_{pp} and $\bar{T}_{\pi p}$ are convenient for numerical calculations, since its oscillations are not so strong.

Appendix C. Covariant basis and Pomeron-Pomeron to di-pion cross-section.

In the classical covariant reggeization as it was considered, for example, in [37], and in author's papers [3], [2], we have the following structure of the amplitudes. Basic elements of such an approach are vertex functions $T^{\mu_1 \dots \mu_J}(p, q)$, where

$$T^{\mu_1 \dots \mu_J}(p, q) = \langle p - q | I^{\mu_1 \dots \mu_J} | p \rangle, \tag{32}$$

hadronic tensor

$$\begin{aligned}
W^{\mu_1 \dots \mu_J \nu_1 \dots \nu_{J'}}(p, q) &= \\
&= \int d^4 x e^{i q x} \langle p | I^{\mu_1 \dots \mu_J}(x) I^{\nu_1 \dots \nu_{J'}}(0) | p \rangle,
\end{aligned} \tag{33}$$

and propagators $\Pi_{\mu_1 \dots \mu_J, \nu_1 \dots \nu_J}(J, t)/(m^2(J) - t)$ with the tensor structure $\Pi_{\mu_1 \dots \mu_J}$ calculated in [37], for example. $1/(m^2(J) - t)$ have the poles at

$$m^2(J) - t = 0, \text{ i.e. } J = \alpha_{\mathbb{P}}(t), \tag{34}$$

after an appropriate analytic continuation of the signatured amplitudes in J . We assume that this pole, where $\alpha_{\mathbb{P}}$ is the Pomeron trajectory, gives, by definition, the dominant contribution at high energies after having taken the corresponding residues. At this stage we do not take into account absorptive corrections (unitarization).

$I^{\mu_1 \dots \mu_J}$ is the current operator related to the hadronic spin- J Heisenberg field operator,

$$(\square + m_J^2) \Phi^{\mu_1 \dots \mu_J}(x) = I^{\mu_1 \dots \mu_J}(x), \tag{35}$$

and

$$\partial_\mu I^{\mu_1 \dots \mu_J} = \partial_\nu I^{\nu_1 \dots \nu_J} = 0; \quad (36)$$

$$I^{\mu_1 \dots \mu_J} = I^{(\mu_1 \dots \mu_J)}; \quad I^{\nu_1 \dots \nu_J} = I^{(\nu_1 \dots \nu_J)}; \quad (37)$$

$$g_{\mu_i \mu_k} I^{\mu_1 \dots \mu_i \dots \mu_k \dots \mu_J} = g_{\nu_i \nu_k} I^{\nu_1 \dots \nu_i \dots \nu_k \dots \nu_J} = 0. \quad (38)$$

In the momentum space Rarita-Schwinger conditions (36)-(38) for the vertex are

$$T^{\mu_1 \dots \mu_i \dots \mu_j \dots \mu_J} = T^{\mu_1 \dots \mu_j \dots \mu_i \dots \mu_J} \quad (39)$$

$$q_{\mu_i} T^{\mu_1 \dots \mu_i \dots \mu_J} = 0 \quad (40)$$

$$g_{\mu_i \mu_j} T^{\mu_1 \dots \mu_i \dots \mu_j \dots \mu_J} = 0, \quad (41)$$

and the same conditions are imposed on each group of indexes in tensors W and Π . Let us note (as was done in [37]), that conditions (39)-(41) are valid only on-mass-shell of the spin-J meson. And when we go to the phase space of the scattering region, these conditions could be relevant only for conserved hadronic currents. However, this may well not be the case.

Let us consider both cases. In the case of conserved currents we can define main transverse structures:

$$\begin{aligned} G_{\alpha\beta} &= g_{\alpha\beta} - \frac{q_\alpha q_\beta}{q^2}; \\ P_\alpha &= \left(p_\alpha - q_\alpha \frac{pq}{q^2} \right) / \sqrt{m^2 - (pq)^2/q^2}, \quad P^2 = 1, \\ K_\alpha &= \left(k_\alpha - q_\alpha \frac{kq}{q^2} \right) / \sqrt{m^2 - (kq)^2/q^2}, \quad K^2 = 1; \\ G_{\alpha\beta} P^\beta &= P_\alpha, \quad G_{\alpha\beta} K^\beta = K_\alpha, \\ g_{\alpha\beta} G^{\alpha\beta} &= G_{\alpha\beta} G^{\alpha\beta} = 3. \end{aligned} \quad (42)$$

For vertex functions T we can obtain the following tensor decomposition:

$$T^{(J)} \equiv T^{\mu_1 \dots \mu_J}(k, q) = F_J(t) \sum_{n=0}^{\lfloor \frac{J}{2} \rfloor} \frac{\mathbb{C}_J^n}{\mathbb{C}_J^0} \left(K^{(J-2n)} G^{(n)} \right), \quad (43)$$

$$\mathbb{C}_J^n = \frac{(-1)^n (2(J-n))!}{(J-n)! n! (J-2n)!}, \quad (44)$$

where tensor structures $(K^{(J-2n)} G^{(n)})^{\mu_1 \dots \mu_J}$ satisfy only two conditions (39), (40) (transverse-symmetric)

$$\left(K^{(J-2n)} G^{(n)} \right) = \frac{K^{(\mu_1 \dots \mu_{J-2n}} G^{\mu_{J-2n+1} \dots \mu_{J-2n+2} \dots \mu_J)}{N_J^n}, \quad (45)$$

$$N_J^n = \frac{J!}{2^n n! (J-2n)!}. \quad (46)$$

Coefficients \mathbb{C}_J^n in (43) can be obtained from the condition (41) which leads to the recurrent set of equations (see [2]). It was also shown in [2], that for elastic scattering of particles with equal masses, which can be obtained by the contraction $T_{\{\mu\}}(p_a, \Delta) \otimes T_{\{\mu\}}(p_b, -\Delta)$,

we have the usual Regge expression for the amplitude. In the general elastic process $a+b \rightarrow c+d$ with unequal masses of particles we can obtain

$$\begin{aligned} \mathcal{M}(s, t) &= T_{\{\mu\}}^{(J)}(p_a, \Delta) \otimes T_{\{\mu\}}^{(J)}(p_b, -\Delta) = \\ &= F_J^{(1)}(t) F_J^{(2)}(t) 2^J \times \\ &\mathcal{P}_J \left(\frac{(s - m_a^2 - m_b^2 + \frac{(m_a^2 - m_c^2 + t)(m_b^2 - m_d^2 + t)}{2t})(-2t)}{\lambda^{1/2}(m_b^2, m_d^2, t) \lambda^{1/2}(m_a^2, m_c^2, t)} \right) \end{aligned} \quad (47)$$

Here the argument of the Legendre function is the t-channel cosine $z_t = \cos \theta_t$, and

$$\lambda(x, y, z) = x^2 + y^2 + z^2 - 2xy - 2xz - 2yz.$$

In the classical Regge scheme

$$\sum_J (2J+1) \mathcal{M}_J \mathcal{P}_J(-z_t) \rightarrow \eta_{\mathbb{R}}(t) \beta_{\mathbb{R}}(t) \left(\frac{s}{s_0} \right)^{\alpha_{\mathbb{R}}(t)}, \quad (48)$$

where we also have Legendre polynomials.

In the case of nonconserved currents we have no Rarita-Schwinger conditions and could propose only some arguments on behaviour of coefficients in tensors

$$T_{\mu_1 \dots \mu_J}^{(J)}(p, q) = \sum_{n+k \leq J} f_J^{n,k} \left\{ p^n q^k g^{[(J-n-k)/2]} \right\}, \quad (49)$$

$$\Pi_{\mu_1 \dots \mu_J, \nu_1 \dots \nu_J} = Q_{(\mu_1 \nu_1 \dots \mu_J \nu_J)} + \text{nonleading}, \quad (50)$$

where

$$\begin{aligned} p^n &= p_{\mu_1} \dots p_{\mu_n}, \quad q^k = q_{\mu_{n+1}} \dots p_{\mu_{n+k}}, \\ g^{[(J-n-k)/2]} &= g_{\mu_{n+k+1} \mu_{n+k+2} \dots \mu_{J-1} \mu_J}, \end{aligned}$$

tensors $\{p^n q^k g^{[(J-n-k)/2]}\}$ and $Q_{(\mu_1 \nu_1 \dots \mu_J \nu_J)}$ are symmetric on μ_i and ν_j groups of indexes. These arguments are

1. all $f_J^{n,k}$ are of the same order of magnitude;
2. tensor Π has the form (50), where

$$Q_{\mu\nu} = g_{\mu\nu} - q_\mu q_\nu / m_J^2,$$

which is equal to $G_{\mu\nu}$ on-mass-shell of the spin-J meson, and other terms in (50) give nonleading contributions to the final result.

In this case we have also simple Regge result like in (48), but without Legendre functions. It is natural to assume, that when spin-J meson is not far from the mass-shell, the structures of vertex and propagator are close to the case of conserved currents.

References

1. R. Ryutin, *Exclusive Double Diffractive Events: general framework and prospects*, Eur. Phys. J. C **73**, 2443 (2013).
2. R. Ryutin, *Visualizations of exclusive central diffraction*, Eur. Phys. J. C **74**, 3162 (2014).
3. V.A. Petrov, R.A. Ryutin, *Single and double diffractive dissociation and the problem of extraction of the proton-Pomeron cross-section*, Int. J. Mod. Phys. A **31**, 1650049 (2016).
4. J.D. Bjorken, *Rapidity gaps and jets as a new-physics signature in very-high-energy hadron-hadron collisions*, Phys. Rev. D **47**, 101 (1993).
5. F. Abe et al. (CDF Collaboration), *Observation of rapidity gaps in $\bar{p} p$ collisions at 1.8 TeV*, Phys. Rev. Lett. **74**, 855 (1995).
6. M.G. Albrow, A. Rostovtsev, *Searching for the Higgs at hadron colliders using the missing mass method*, FERMILAB-PUB-00-173 (2000), arXiv: 0009336[hep-ph].
7. L.A. Harland-Lang, V.A. Khoze, M.G. Ryskin, *Central exclusive production and the Durham model*, Int. J. Mod. Phys. A **29**, 1446004 (2014).
8. L.A. Harland-Lang, V.A. Khoze, M.G. Ryskin, W.J. Stirling, *Central exclusive production within the Durham model: a review*, Int. J. Mod. Phys. A **29**, 1430031 (2014).
9. L.A. Harland-Lang, V.A. Khoze, M.G. Ryskin, *Modeling exclusive meson pair production at hadron colliders*, Eur. Phys. J. C **74**, 2848 (2014).
10. P. Lebiedowicz, O. Nachtmann, A. Szczurek, *Tensor pomeron, vector odderon and diffractive production of meson and baryon pairs in proton-proton collisions*, EPJ Web Conf. **206**, 06005 (2019).
11. P. Lebiedowicz, O. Nachtmann, A. Szczurek, *Exclusive diffractive production of $\pi^+\pi^-$ continuum and resonances within tensor pomeron approach*, EPJ Web Conf. **130**, 05011 (2016).
12. P. Lebiedowicz, A. Szczurek, *Revised model of absorption corrections for the $pp \rightarrow p\pi^+\pi^-p$ process*, Phys. Rev. D **92**, 054001 (2015).
13. R. Waldi, K.R. Schubert and K. Winter, *Search for glueballs in a pomeron pomeron scattering experiment*, Z. Phys. C **18**, 301 (1983).
14. A. Breakstone et al. (ABCDHW Collaboration), *The reaction Pomeron-Pomeron $\rightarrow \pi^+\pi^-$ and an unusual production mechanism for the $f_2(1270)$* , Z. Phys. C **48**, 569 (1990).
15. L. Adamczyk, W. Guryn and J. Turnau, *Central exclusive production at RHIC*, Int. J. Mod. Phys. A **29**, 1446010 (2014).
16. R. Sikora, *Central Exclusive Production of meson pairs in proton-proton collisions at $\sqrt{s} = 200$ GeV in the STAR experiment at RHIC*, talk at Low x Meeting, 1-5 September 2015, Sandomierz, Poland.
17. T.A. Aaltonen et al. (CDF Collaboration), *Measurement of central exclusive $\pi^+\pi^-$ production in $p\bar{p}$ collisions at $\sqrt{s} = 0.9$ and 1.96 TeV at CDF*, Phys. Rev. D **91**, 091101 (2015).
18. M. Albrow, J. Lewis, M. Zurek, A. Swiech, D. Lontkovskyi, I. Makarenko and J.S. Wilson, the public note called *Measurement of Central Exclusive Hadron Pair Production in CDF* is available at <http://www-cdf.fnal.gov/physics/new/qcd/GXG.14/webpage/>.
19. CMS Collaboration, *Measurement of exclusive $\pi^+\pi^-$ production in proton-proton collisions at $\sqrt{s} = 7$ TeV*, CMS-PAS-FSQ-12-004.
20. K. Osterberg, *Potential of central exclusive production studies in high β^* runs at the LHC with CMS-TOTEM*, Int. J. Mod. Phys. A **29** 1446019 (2014).
21. A.A. Godizov, *Effective transverse radius of nucleon in high-energy elastic diffractive scattering*, Eur. Phys. J. C **75**, 224 (2015).
22. A.A. Godizov, *Asymptotic properties of Regge trajectories and elastic pseudoscalar-meson scattering on nucleons at high energies*, Yad. Fiz. **71**, 1822 (2008).
23. J.R. Pelaez, A. Rodas, J. Ruiz De Elvira, *Global parameterization of $\pi\pi$ scattering up to 2 GeV*, e-Print: arXiv:1907.13162 [hep-ph].
24. A.A. Godizov, *Current stage of understanding and description of hadronic elastic diffraction*, AIP Conf.Proc. **1523**, 145 (2013).
25. V.A. Petrov, *High-energy implications of extended unitarity*, IFVE-95-96, IHEP-95-96, talk given at Blois Conference: 20-24 Jun 1995, Blois, France
26. V.A. Petrov, R.A. Ryutin, A.E. Sobol and J.-P. Guillaud, *Azimuthal angular distributions in EDDE as spin-parity analyser and glueball filter for LHC*, JHEP **0506**, 007 (2005).
27. A.A. Godizov, *High-energy central exclusive production of the lightest vacuum resonance related to the soft Pomeron*, Phys. Lett. B **787**, 188 (2018).
28. A.B. Kaidalov and K.A. Ter-Martirosyan, *The pomeron-particle total cross-section and diffractive production of showers at very high energies*, Nucl. Phys. B **75**, 471 (1974).
29. A.B. Kaidalov, *Diffractive Production Mechanisms*, Phys. Rept. **50**, 157 (1979).
30. N. Agababyan et al. (EHS/NA22 Collaboration), *Pomeron-pomeron cross-section from inclusive production of a central cluster in quasi-elastic $\pi^+ p$ and $K^+ p$ scattering at 250 GeV/c*, Z. Phys. C **60**, 229 (1993).
31. R.A. Buchl and B.P. Nigam, *Possible Behavior of Pomeron-Pomeron Total Cross Section*, Prog. Theor. Phys. **55**, 1879 (1976).
32. K.H. Streng, *Pomeron-Pomeron collisions at collider energies*, Phys. Lett. B **166**, 443 (1986).
33. C.G. Roldao and A.A. Natale, *Photon-Photon and Pomeron-Pomeron Processes in Peripheral Heavy Ion Collisions*, Phys. Rev. C **61**, 064907 (2000).
34. N. Armesto and M.A. Braun, *The pomeron-pomeron interaction in the perturbative QCD*, Phys. Lett. B **385**, 284 (1996).
35. R.A. Ryutin, *Total pionproton cross-section from the new LHCf data on leading neutrons spectra*, Eur. Phys. J. C **77**, 114 (2017); Erratum: Eur. Phys. J. C **77**, 843 (2017).
36. R.A. Ryutin, *ExDiff Monte Carlo generator for Exclusive Diffraction. Version 2.0. Physics and manual*, e-Print: arXiv:1805.08591 [hep-ph]
37. R.L. Ingraham, *Covariant Propagators and Vertices for Higher Spin Bosons*, Prog. Theor. Phys. **51**, 249 (1974).